

Electron-beam propagation in a two-dimensional electron gas

E. G. Novik, H. Buhmann, and L. W. Molenkamp

Physikalisches Institut der Universität Würzburg, Am Hubland, 97074 Würzburg, Germany

(Dated: November 16, 2018)

A quantum mechanical model based on a Green's function approach has been used to calculate the transmission probability of electrons traversing a two-dimensional electron gas injected and detected via mode-selective quantum point contacts. Two-dimensional scattering potentials, back-scattering, and temperature effects were included in order to compare the calculated results with experimentally observed interference patterns. The results yield detailed information about the distribution, size, and the energetic height of the scattering potentials.

PACS numbers: 72.20.Dp, 73.23.Ad, 71.55.Eq

I. INTRODUCTION

The electron mobility in a two-dimensional electron gas (2DEG) is limited by electron-impurity scattering [1, 2, 3]. The impurity potential originates mainly from ionized donors located in the remote doping layer. However, the observed high mobilities can only be explained when correlations of different donor states are taken into account [4, 5]. Up to now experiments are rare which probe the actual impurity potential microscopically. Standard transport experiments yield only information about the averaged potential fluctuations by defining the average electron mean free path. Recently, it has been shown that the electrons injected via quantum point contacts (QPC) into a 2DEG can be used as a local probe for these scattering potentials either through the interference patterns observed in the transmission probability [6] or through structures in the position dependent electron reflection [7, 8].

In this paper we use a Green's function approach to calculate the transmission probability of electrons injected via QPC into a 2DEG exposed to a small magnetic field. The results are compared with experimentally observed transmission probabilities where the electrons were detected with a second QPC in a distance of $4\ \mu\text{m}$ opposite to the injector QPC. In order to reproduce the experimental results the shape, size, and height of scattering potentials has been modeled and back-scattering as well as temperature effects have been included into these calculations.

II. MODEL

Our model is adopted to the experimental situation presented in Fig. 1 a) (c.f. Ref. [6]). This figure shows two opposite QPCs in a distance L from each other. In the experiment these QPCs are formed electrostatically in the 2DEG of GaAs/Al_{0.33}Ga_{0.67}As-heterostructure by externally controlled Schottky gates (gray areas). Due to the saddle-point-like electrostatic potential of the QPCs in the plane of the 2DEG the electrons are injected into the region between the two QPCs in form of a collimated beam [9]. A weak magnetic field, applied perpendicular

to the plane of the 2DEG, deflects the electrons and the resulting signal of the electrons which reach the detector QPC is proportional to the profile of the propagated electron beam. It has been shown in Ref. [6] that the observed structure in the electron beam signal is due to electron interference effects, which originate from scattering at potential fluctuations imposed into the 2DEG from donors in different charged states. A typical experimental result is shown in Fig. 2 (curves E).

The first attempt to calculate the transmission probability of an electron beam injected by a QPC into a 2DEG and detected by a second opposite QPC was made by M. Saito *et al.* [10] using a Green's function approach. This approach was previously extended by us in order to include interference effects due to electron impurity scattering [6]. The scattering potential has been treated in a very simplified way by setting the part of a wave function at the impurity position to zero (infinite impurity potential), which explained the experimental data qualitatively. Here, we present quantum mechanical calculations which include a realistic two-dimensional impurity potential model as well as back-scattering and temperature effects. A fitting to the experimental data yields information about the distribution, size and strength of scattering potentials in a 2DEG. In contrast to our previous work [6], finite potential fluctuations with positive and negative heights (counted from the bottom of the conduction band) are considered, corresponding to the regions of reduced and increased electron density, respectively. Moreover, the back-scattering effects from the impurity potentials and sample boundaries were taken into account. It turns out that the back-scattering affects the interference patterns considerably in two cases: first, if the impurity is located close to the injector or the detector QPC (within the phase coherence length), or second, if two impurities are located at a short distance from each other. The effect is stronger when the scattering potential is significantly higher than the Fermi energy. Finally, temperature effects are considered, i.e., a thermal averaging of the propagated beam is included [11], as well as the contribution from electron-electron scattering [12].

The following initial parameters are set according to the experimental situation for the calculations: the distance (L) between the two QPCs is $4\ \mu\text{m}$, which is smaller

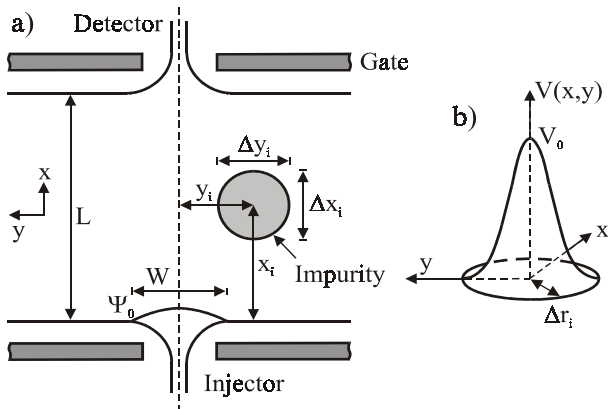


FIG. 1: a) Scheme of the sample structure used for the calculations (Ψ_0 - the wave function at the exit of injector quantum point contact); b) the shape of the scattering potential.

than the elastic mean free path, the electron mobility and carrier density are $\mu \approx 100 \text{ m}^2/\text{Vs}$ and $n_s \approx 2 \times 10^{15} \text{ m}^{-3}$, respectively, and the width (W) of the QPC's exit is 100 nm accounting for a single mode electron injection in case of an adiabatic expansion [6, 9]. The wave function propagation is perturbed by potential fluctuations, which are described in the following way: x_i , y_i , and Δx_i , Δy_i define the position and extension in the x - y plane and $V(x, y)$ the potential height (Fig. 1). It was found that in most cases circular impurities ($\Delta x_i = \Delta y_i$) are sufficient to produce a good agreement between the calculations and the experiments. Hence, we restrict ourself in this paper to the presentation of results considering only circular impurity potentials with a radius which is given by $\Delta r_i = \sqrt{\Delta x_i^2/4 + \Delta y_i^2/4}$.

Our model numerically solves the time-independent Schrödinger equation for a static magnetic field [10]. Using the Green's function method with Dirichlet's boundary conditions it is possible to evaluate the wave function for a line at any distance x' from the injector, according to [10]:

$$\Psi(x', y') = \frac{\hbar}{2m^*} \int_{-W/2}^{W/2} \Psi_B(0, y) \left. \frac{\partial G^+}{\partial x} \right|_{x=0} dy. \quad (1)$$

Here, Ψ_B is the wave function at the injector QPC exit which includes the effect of the magnetic field in the form of the phase shift Θ_0 between the center and any point on the QPC exit:

$$\Psi_B(0, y) = \Psi_0(0, y) \exp[i\Theta_0(y)], \quad (2)$$

Ψ_0 is the wave function at the injector QPC exit without magnetic field and G^+ is the Green's function calculated in a weak-magnetic-field approximation using the mirror-image method. For a detailed description of this method we refer to Ref. [10]. The unperturbed wave

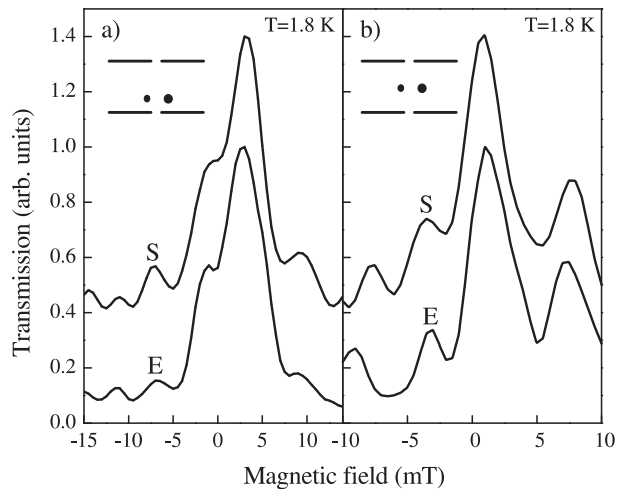


FIG. 2: Measured electron beam profiles (curves E) and calculated interference patterns (curves S) for two scattering potentials versus magnetic field (simulation results are presented with a shift). Parameters for the scattering potentials are: a) $x_i = 1.3 \mu\text{m}$, $y_i = -0.34 \mu\text{m}$, $\Delta r_i = 0.045 \mu\text{m}$, $V_0 \approx 33 \text{ meV}$ for first impurity and $x_i = 1.3 \mu\text{m}$, $y_i = 0.18 \mu\text{m}$, $\Delta r_i = 0.075 \mu\text{m}$, $V_0 \approx 16 \text{ meV}$ for second; b) $x_i = 2 \mu\text{m}$, $y_i = -0.42 \mu\text{m}$, $\Delta r_i = 0.05 \mu\text{m}$, $V_0 \approx 8 \text{ meV}$ for first impurity and $x_i = 2 \mu\text{m}$, $y_i = 0.215 \mu\text{m}$, $\Delta r_i = 0.075 \mu\text{m}$, $V_0 \approx 10 \text{ meV}$ for second.

function can be calculated for the whole 2DEG area between injector and detector. However, in the region $x_i - \Delta r_i < x < x_i + \Delta r_i$, $y_i - \Delta r_i < y < y_i + \Delta r_i$ the wave function propagation is perturbed by a scattering potential. One suitable approximation for the shape of this potential is a hyperbolic function [13], which is very similar to a Gaussian potential commonly used in literature for the description of the effective potential due to remote charged donors in the 2DEG region [14]. A hyperbolic potential has the advantage that the solution for the transmission and reflection coefficients can be obtained analytically [13]. The scattering potential is given by [Fig. 1 b)]:

$$V(x, y) = V_0 \cosh^{-2} \left[\frac{\sqrt{(y - y_i)^2 + (x - x_i)^2}}{a \Delta r_i} \right], \quad (3)$$

V_0 defines the height of the potential which can be positive and negative depending on its relative height compared to the bottom of the conduction band for the average carrier density [15]. The constant a has been chosen $a \approx 0.4$ in order to allow for the following approximation: $V(x, y) \approx 0$ for $\sqrt{(y - y_i)^2 + (x - x_i)^2} > \Delta r_i$, i.e. the impurity potential acts as a local perturbation.

The effect of the scattering potential is calculated in the following way: first, the unperturbed wave function is calculated for a line $x = x_i + \Delta r_i$ behind the impurity potential. Then the transmission probability of this scatterer is evaluated and the resulting wave function at

$x = x_i + \Delta r_i$ is calculated from:

$$\Psi_T(x_i + \Delta r_i, y) = \Psi(x_i + \Delta r_i, y) t(y), \quad (4)$$

where $\Psi(x_i + \Delta r_i, y)$ is the wave function, calculated omitting the impurity. As long as the size of the scattering potential is much smaller than the distance between injector and detector QPC, the transmission amplitude can be calculated from:

$$t(y) = \frac{\Gamma(-i\bar{k} - s(y)) \Gamma(-i\bar{k} + s(y) + 1)}{\Gamma(1 - i\bar{k}) \Gamma(-i\bar{k})}, \quad (5)$$

where

$$s(y) = \frac{1}{2} \left(-1 + \sqrt{1 - \frac{8m^*V(x_i, y)}{(\hbar/a\Delta)^2}} \right), \quad (6)$$

and

$$\bar{k} = ka\Delta, \quad (7)$$

where Γ is the gamma function, $k = \frac{\sqrt{2m^*E}}{\hbar}$; $V(x_i, y)$ is the height of the impurity at the position y [Eq. (3)]; $\Delta = \sqrt{\Delta r_i^2 - (y_i - y)^2}$ (where $|y - y_i| < \Delta r_i$) is the half of the extension of the impurity in x -direction for a given y -coordinate. Multiple impurity potentials are considered in the same successive way. The modified wave function is then used to calculate the wave function at the detector position ($x = L$) using Eq. (1). The transmission coefficient for the detector QPC is calculated from

$$T = \left| \int_{-W/2}^{W/2} \Psi_D^*(L, y') \Psi(L, y') dy' \right|^2, \quad (8)$$

where $\Psi_D(L, y')$ is the wave function in the detector QPC, which is taken in analogy to the wave function Ψ_B at the exit of the injector QPC [6].

From comparing the calculated transmission probability with the measured beam profile it is possible to determine the parameters of the scattering potential. As an example two experimental traces and matching theoretical results are presented in Fig. 2. Good agreement is obtained for both cases when two scattering potentials are introduced into the region between injector and detector. The sizes of the impurities are comparable with Fermi wavelength $\lambda_F \approx 0.05 \mu\text{m}$, and their heights are equal or exceed Fermi energy $E_F \approx 8 \text{ meV}$.

The sensitivity of the interference pattern to the parameters of the scattering potential is demonstrated in Fig. 3 for the case of a single impurity. The initial parameters (location $x_i = 2 \mu\text{m}$, $y_i = 0.205 \mu\text{m}$, size $\Delta r_i = 0.035 \mu\text{m}$ and height $V_0 \approx 16 \text{ meV}$) were those which give the best fit of the experimental data presented

in Fig. 4 (curve E). In Fig. 3 a) the influence of the parameter x_i on the interference pattern is demonstrated: if the impurity is located far away from the injector QPC (and detector), e.g. $x_i = L/2$, the observed interference patterns are relative insensitive to small changes in x_i . A change of about 20% is needed to give the result shown in Fig. 3 a) trace 2. However, if the impurity is located much closer either to injector or detector [Fig. 3 a) trace 3], changes in x_i of 5% result in a similar strong effect (trace 4) as observed for the center position. The influence of the parameter y_i is strong but only weakly dependent on the x -position: changes of y_i by 5% lead to shifts of the interference maxima by 1 – 6% [traces 2 and 3 in Fig. 3 b)]. Fig. 3 c) shows the sensitivity of the interference patterns to the variation of the parameter Δr_i by 10%. The interference maxima for curves 2 and 3 are shifted relative to the initial curve by 1 – 4%, which demonstrates also here the relatively high sensitivity of the fitting procedure. The influence of the parameter V_0 is quite different depending on the absolute height compared with the Fermi energy. Two examples are given in Fig. 3 d) where the interference patterns for $V_0 \approx 16 \text{ meV}$ (trace 1) and $V_0 \approx 7.3 \text{ meV}$ (trace 3) are shown. The lower potential height corresponds closely to the Fermi energy. It can be seen that a change of V_0 of 25% (trace 2) in the first case ($V_0 > E_F$) is needed to achieve a similar deviation from the initial curve as it has been obtained for a change of only 10% (trace 4) in the case when V_0 is comparable to E_F .

It should be noted that the simulations do exhibit an ambiguity in the determination of the impurity position in the direction of electron beam propagation (i.e. in the determination of the position x_i). Because of the symmetry of the device, a similar transmission probability results for an impurity located at a distance x_i or $x'_i \approx L - x_i$ from the injector QPC boundaries, when the other impurity parameters are kept constant. A further ambiguity is in the determination of the character of the scattering potential, i.e., it is possible to obtain similar interference patterns for a barrier ($V_0 > 0$) and for a dip ($V_0 < 0$). In Fig. 4 the calculated transmission probability for a potential barrier (curve B1) and a dip (curve D2) are shown. The results reproduce the characteristic features of the experimental data quite well. The scatterers have in both cases a radius $\Delta r_i = 0.035 \mu\text{m}$ but they differ in position and height. Optimal locations found in the simulation were $x_i = 2 \mu\text{m}$, $y_i = 0.205 \mu\text{m}$ for the potential barrier and $x_i = 2 \mu\text{m}$, $y_i = 0.24 \mu\text{m}$ for the dip, for potential heights are $V_0 \approx 16 \text{ meV}$ and $V_0 \approx -14 \text{ meV}$, respectively. It can be seen that a simple change of the sign of the potential height does not result in satisfying fitting of the experimental data. Fig. 4 shows the inversion from a barrier (curve B1) into a dip (curve D1) and from a dip (curve D2) into a barrier (curve B2). From these results it can be seen, that the absolute value of this fitting parameter depends mainly on the choice of the character of the scattering potential (dip or barrier). However, for most of our calculations we decided on bar-

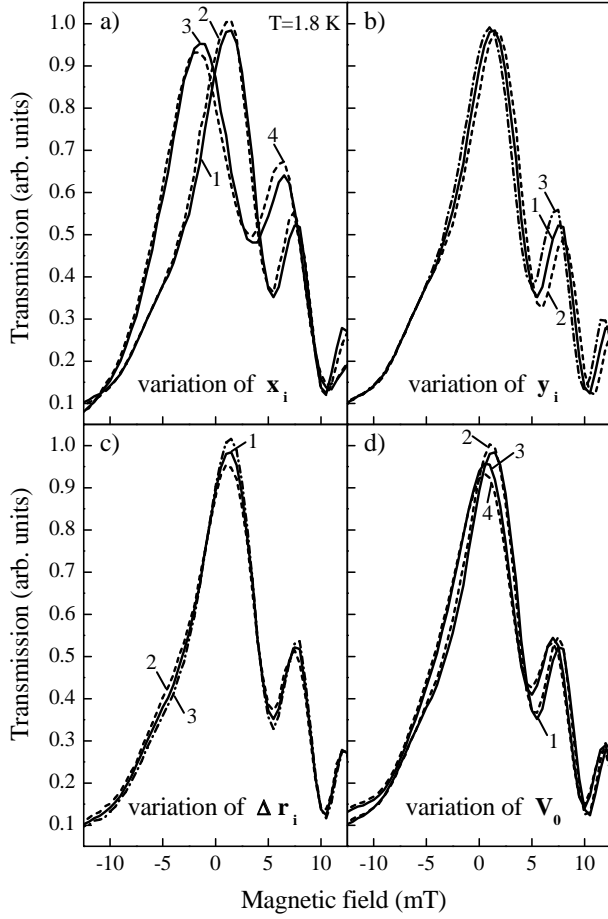


FIG. 3: Calculated interference patterns for different values of the impurity potential parameters. Curve 1 in all for figures: $x_i = 2 \mu\text{m}$, $y_i = 0.205 \mu\text{m}$, $\Delta r_i = 0.035 \mu\text{m}$, $V_0 \approx 16 \text{ meV}$; a) $x_i = 2.4 \mu\text{m}$ (curve 2), $x_i = 0.6 \mu\text{m}$ (curve 3) and $x_i = 0.57 \mu\text{m}$ (curve 4); b) $y_i = 0.195 \mu\text{m}$ (curve 2) and $y_i = 0.215 \mu\text{m}$ (curve 3); c) $\Delta r_i = 0.031 \mu\text{m}$ and $\Delta r_i = 0.039 \mu\text{m}$ (curve 3); d) $V_0 \approx 12 \text{ meV}$ (curve 2), $V_0 \approx 7.3 \text{ meV}$ (curve 3) and $V_0 \approx 6.5 \text{ meV}$ (curve 4).

rier type potentials which correspond to 2DEG areas of reduced carrier density. In real GaAs 2DEG structures this type of scattering potentials is expected due to the formation of negatively charged DX centers in the remote donor layer [5].

So far we have not taken into account any temperature effects. Experimentally the interference patterns have been observed to smear out with increasing temperature, practically disappearing at $T \approx 4 \text{ K}$ [Fig. 5 a)]. We first consider thermal broadening as the origin of this behavior. The detector signal results from electrons with different energies $E_F \pm k_B T$ propagating from injector to detector. In order to include this effect the calculations of the wave function [Eqs. (1, 4-7)] were carried out for the corresponding values of wave vector $k = \frac{\sqrt{2m^*(E_F \pm k_B T)}}{\hbar}$. The thermally averaged transmission probability is then

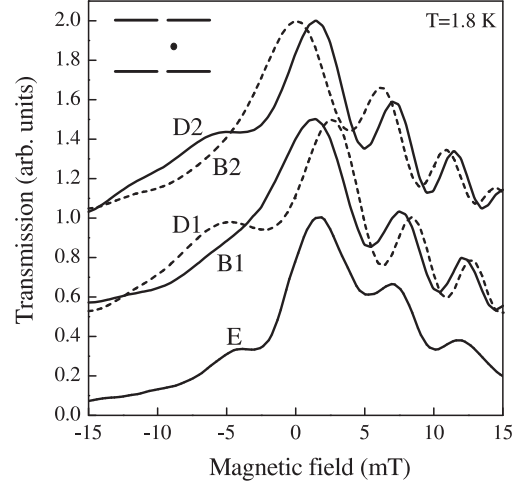


FIG. 4: Calculated interference patterns for a barrier (curves B1 and B2) and for a dip (curves D1 and D2) in comparison with experimental data (curve E). All characteristics are normalized with respect to the maximum transmission value. Results are displayed with a constant shift for clarity. Parameters for the impurities are: $x_i = 2 \mu\text{m}$, $y_i = 0.205 \mu\text{m}$, $\Delta r_i = 0.035 \mu\text{m}$, $V_0 \approx 16 \text{ meV}$ (curve B1); $x_i = 2 \mu\text{m}$, $y_i = 0.205 \mu\text{m}$, $\Delta r_i = 0.035 \mu\text{m}$, $V_0 \approx -16 \text{ meV}$ (curve D1); $x_i = 2 \mu\text{m}$, $y_i = 0.24 \mu\text{m}$, $\Delta r_i = 0.035 \mu\text{m}$, $V_0 \approx 14 \text{ meV}$ (curve B2); $x_i = 2 \mu\text{m}$, $y_i = 0.24 \mu\text{m}$, $\Delta r_i = 0.035 \mu\text{m}$, $V_0 \approx -14 \text{ meV}$ (curve D2).

calculated as:

$$T = \left| \int -\frac{\partial f(E)}{\partial E} \left[\int_{-W/2}^{W/2} \Psi_D^*(L, y') \Psi(L, y', E) dy' \right] dE \right|^2, \quad (9)$$

where $-\frac{\partial f(E)}{\partial E}$ is the derivative of the Fermi function [11]. From Fig. 5 b) it can be seen that the reduction of the amplitude of the detector signal with increasing temperature is reasonably reproduced by the thermal broadening. However, the signal still shows all features corresponding to the low temperature interference patterns [Fig. 5 b) solid lines], while experimentally these features are all smeared out. This result implies that further temperature effects are responsible for the experimental observations. Another phenomenon which strongly influences the appearance of interference effects in an electron system is electron-electron scattering. It leads to a dephasing of electrons but leaves their trajectories due to phase space restraints in a 2D system practically unaffected [12]. As long as the electron-electron scattering mean free path l_{ee} is larger than the distance between QPCs L we can use a one-collision approximation to consider this effect [12], i.e. an electron that has been scattered is unlikely to be scattered again before it reaches the detector. It has been shown [12] that the contribution of electrons that reach the detector ballistically can be approximated by:

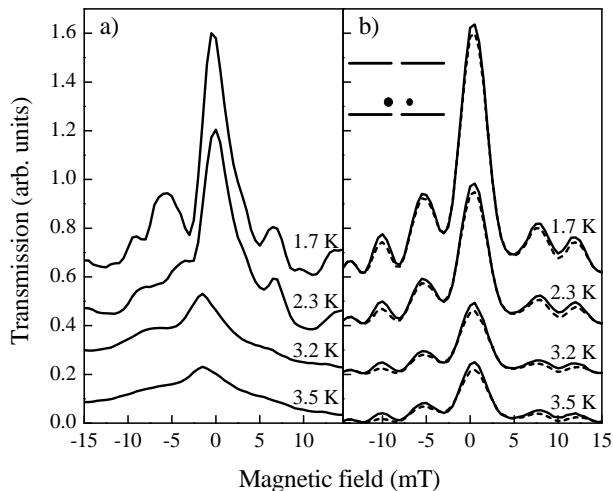


FIG. 5: Measured electron beam profiles (a) and calculated interference patterns (b) at different temperatures (solid lines: only thermal broadening is considered, dashed lines: thermal broadening and electron-electron scattering effects are included). Results are displayed with a constant shift for clarity. Parameters for the scattering potentials are: $x_i=1.2 \mu\text{m}$, $y_i = -0.26 \mu\text{m}$, $\Delta r_i = 0.08 \mu\text{m}$, $V_0 \approx -8 \text{ meV}$ for first impurity (dip) and $x_i = 1.2 \mu\text{m}$, $y_i = 0.23 \mu\text{m}$, $\Delta r_i = 0.04 \mu\text{m}$, $V_0 \approx 82 \text{ meV}$ for second (barrier).

$$\Psi_b(L, y) = \Psi(L, y) \exp\left(-\frac{L}{l_{ee}}\right), \quad (10)$$

where l_{ee} is determined using the usual expression for the energy relaxation length in a 2DEG [16]:

$$l_{ee} = v_F \tau_{ee},$$

$$\frac{1}{\tau_{ee}} = -\frac{E_F}{4\pi\hbar} \left(\frac{\Delta}{E_F}\right)^2 \left[\ln\left(\frac{\Delta}{E_F}\right) - \ln\left(\frac{2 q_{TF}}{k_F}\right) - \frac{1}{2} \right], \quad (11)$$

where $v_F = \sqrt{\frac{2E_F}{m^*}}$ is the Fermi velocity, τ_{ee} is the electron-electron scattering time, Δ is the electron excess energy relative to E_F , q_{TF} is the 2D Thomas-Fermi screening wave vector, and $k_F = \frac{\sqrt{2m^*E_F}}{\hbar}$. Electrons that have been scattered lose their phase information, and reach the detector with an arbitrary phase. Their contribution to the transmitted signal can be expressed as:

$$\Psi_s(L, y) = \Psi^0(L, y) \left[1 - \exp\left(-\frac{L}{l_{ee}}\right) \right], \quad (12)$$

where $\Psi^0(L, y)$ is the wave transmitted from injector to detector QPC without impurities in the channel [Eq. (1)]. The total propagated signal is then determined as the

sum of Eq. (10) and Eq. (12). The results of this calculation are presented in Fig. 5 b) (dashed lines) for different temperatures from 1.7 K to 3.5 K. It can be seen that the effect of electron-electron scattering contributes to a further decrease and smearing of the interference pattern [Fig. 5 b), dashed lines]. However, even at 3.5 K the structure is still more pronounced than experimentally observed. We conclude that even more dephasing processes contribute to the experimental data, e.g., electron-phonon scattering processes, which have not been considered in our model.

Up to now only forward propagating electrons have been considered in the calculations. However, electrons that are scattered out of the beam can be scattered again by an additional impurity potential or the system boundaries and then reach the detector. For a complete simulation of the device behavior these back-scattered electrons have also to be considered in the calculations. Since back-scattered electrons travel much longer distances before they reach the detector, the effect has to be taken into account only if the additional path length remains smaller than the electron-electron scattering length, i.e. smaller than the phase coherence length. For temperatures considered here, this holds only for back-scattering effects that occur at scattering centers located in close vicinity to the injector or detector, or if two scattering potentials are close to each other. If the impurity is located near the injector, the back-scattered wave must be calculated as that part of the injected beam that is scattered from the impurity towards the injector QPC, reflected at the injector boundaries, and then retransmitted via the impurity towards the detector QPC. For this configuration, self-consistent calculations of the modified injected electron beam $\Psi(0)'$ due to back-scattered electrons into the injector QPC should be used in the simulation. We have not attempted to incorporate such self-consistency into our model. However, a self-consistent method is not needed when the impurity is located near the detector. In this case, the back-scattered wave is that part of the beam that is reflected back from the channel boundaries near the detector towards the impurity and subsequently is scattered into the detector QPC. The calculated transmission probabilities without and with back-scattering effects for a temperature of $T=1.8 \text{ K}$ are presented in Fig. 6 a) for the case of an impurity located near detector QPC. It can be seen that for different values of x_i the interference patterns are very similar when back-scattering is omitted (lower curves in Fig. 6 a), and that the curves differ significantly when back-scattering is taken into account (upper curves in Fig. 6 a). To illustrate this effect more clearly, a part of the upper trace in Fig. 6 a) is replotted enlarged in Fig. 6 b) (solid line). It can be seen that if the initial position of the scattering potential is changed by an amount of the order of $\lambda_F/4$ (Fermi wavelength $\lambda_F \approx 50 \text{ nm}$ for the samples under investigation), structures in the electron beam signal which appeared as a maximum in the initial curve are rendered into a minimum and vice versa. The initial shape is re-

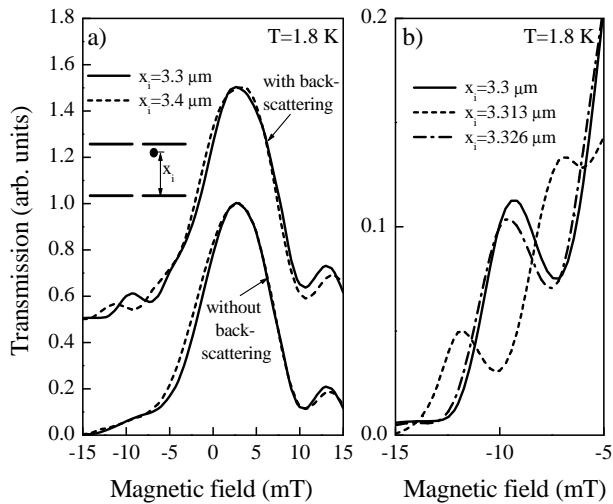


FIG. 6: a) Calculated interference patterns without and with consideration of the back-scattering effects. Parameters for the scattering potential are: $x_i = 3.3 \mu\text{m}$ for solid lines and $x_i = 3.4 \mu\text{m}$ for dashed lines, $y_i = 0.15 \mu\text{m}$, $\Delta r_i = 0.075 \mu\text{m}$, $V_0 \approx 41 \text{ meV}$ (the results including back-scattering are presented with a shift). b) Enlarged section of the upper trace in Fig. a) for three different values of x_i : $3.3 \mu\text{m}$ (solid line), $3.313 \mu\text{m}$ (dashed line), $3.326 \mu\text{m}$ (dot-dashed line).

covered if the position is changed by $\approx \lambda_F/2$. This effect, which obviously results for constructive and destructive interferences, directly manifests the wave nature of the electron beam.

Our calculations enable us not only to understand electron beam collimation experiments, but are applicable also to recent experiments where an electron beam in the vicinity of a QPC has been manipulated by a charged tip of an atomic force microscope [7, 8]. The tip of the microscope introduces a scattering potential which can be located anywhere in the 2DEG area. Electrons which are back-scattered into the injector are detected via changes in the injector current. These changes can be used to map out the current distribution behind the injector QPC. The effect of coherent constructive and destructive interference of back-scattered electrons [Fig. 6 b)] is clearly demonstrated in these experiments. However, in our opinion the authors' conclusion of a branching of the electron beam around the scattering potentials is a misinterpretation. An experimental absence of current variation at the injector QPC does not imply that the current density is zero at the point where the atomic force microscope tip is located. Especially when the charged tip is behind a potential fluctuation of the 2DEG layer no noticeable changes are expected in the injector current. Based on our simulation, we surmise that in this situation when the tip and the scatterer are located close to each other

multiple back-scattering events have to be considered, which drastically reduce the number of electrons reaching the injector QPC. Therefore, from this observation no information on the propagating electron beam can be obtained. Furthermore, a branching of the electron beam can be excluded due to numerous electron beam collimation experiments using a second QPC as detector for the actual electron beam [8, 9, 17, 18, 19] at distances of up to $4 \mu\text{m}$. In none of these experiments 'dark' areas have been detected. The center part of the beam exhibits always the highest signal intensity and observed structures are well explained by wave interference effects. It should be noted that the Fraunhofer diffraction picture is not sufficient to reproduce the observed inference patterns in electron beam experiments. A fully quantum mechanical model is needed, as we have demonstrated here.

III. CONCLUSION

In this paper we presented a comprehensive quantum mechanical model to calculate the transmission probability of an electron beam traversing a 2DEG region confined between two opposite electrostatically defined QPCs. By including local potential fluctuations, temperature and geometric effects experimental results can be interpreted in great detail. The main features of the experimental data are represented in the calculation already including only one or two locations for a circular shaped scattering potentials. Even though interpretation of the values given for the location is sometimes ambiguous due to the symmetry of the system, the extracted sizes and strengths exhibit only a few percent of uncertainty and give for the first time reliable values for the dimensional extents and strengths. It should be noted here that this symmetry is broken when back-scattering and a finite mean free path are fully taken into account. The extracted dimensions and amplitudes of the scattering centers correspond well with estimations from first principle calculations on the correlation of remote donors (size: [4], strength: [15]). Also modulation of QPC currents in local probe experiments can be completely understood in terms of back-scattered electrons from a scattering potential induced by the charged local probe.

Acknowledgments

We acknowledge support by the Alexander von Humboldt foundation, the German Academic Exchange Service (DAAD), and the Deutsche Forschungsgemeinschaft (SFB 410).

[1] E. Buks, M. Heiblum, and H. Shtrikman, Phys. Rev. B **49**, 14790 (1994).

[2] A. L. Efros, F. G. Pikus, and G. G. Samsonidze, Phys.

- Rev. B **41**, 8295 (1990).
- [3] M. Hayne, A. Usher, J. J. Harris, V. V. Moshchalkov, and C. T. Foxon, Phys. Rev. B **57**, 14813 (1998).
- [4] J. A. Nixon and J. H. Davies, Phys. Rev. B **41**, 7929 (1990).
- [5] D. J. Chadi and K. J. Chang, Phys. Rev. Lett. **61**, 873 (1988).
- [6] J. J. Koonen, H. Buhmann, and L. W. Molenkamp, Phys. Rev. Lett. **84**, 2473 (2000).
- [7] M. A. Topinka, B. J. LeRoy, R. M. Westervelt, S. E. J. Shaw, R. Fleischmann, E. J. Heller, K. D. Maranowski, and A. C. Gossard, Nature **410**, 183 (2001).
- [8] R. Crook, C. G. Smith, C. H. W. Barnes, M. Y. Simmons, and D. A. Ritchie, J. Phys.: Condens. Matter **12**, L167 (2000).
- [9] L. W. Molenkamp, A. A. M. Staring, C. W. J. Beenakker, R. Eppenga, C. E. Timmering, and J. G. Williamson, Phys. Rev. B **41**, 1274 (1990).
- [10] M. Saito, M. Takatsu, M. Okada, and N. Yokoyama, Phys. Rev. B **46**, 13220 (1992).
- [11] S. E. J. Shaw, R. Fleischmann, and E. J. Heller, arXiv:cond-mat/0105354.
- [12] A. V. Yanovsky, H. Predel, H. Buhmann, R. N. Gurzhi, A. N. Kalinenko, A. I. Kopeliovich, and L. W. Molenkamp, Europhys. Lett. **56**, 709 (2001).
- [13] A. Galindo and P. Pascual, *Quantum Mechanics II* (Springer-Verlag, Berlin, 1991), p. 109.
- [14] D. Liu and S. D. Sarma, Phys. Rev. B **51**, 13821 (1995).
- [15] I. A. Larkin, J. H. Jefferson, and A. V. Vagov, Physica E **12**, 699 (2002).
- [16] G. F. Giuliani and J. J. Quinn, Phys. Rev. B **26**, 4421 (1982).
- [17] Y. Takagaki, K. Gamo, S. Namba, S. Ishida, S. Takaoka, K. Murase, K. Ishibashi, and Y. Aoyagi, Solid State Commun. **68**, 1051 (1988).
- [18] G. Timp, R. Behringer, S. Sampere, J. E. Cunningham, and R. E. Howard, in *Nanostructure Physics and Fabrication*, edited by M. Reed and W. P. Kirk (Academic Press, New York, 1989), p. 331.
- [19] M. Okada, M. Saito, M. Takatsu, K. Kosemura, T. Nagata, H. Ishiwari, and N. Yokoyama, Superlatt. Microstruct. **10**, 493 (1991).